High-Capacity Reversible Lithium Storage in Defined Microporous Carbon Framework for All Solid-State Lithium Batteries

Luise Maria Bloi[a,b], Felix Hippauf[b], Tom Boenke[a,b], Marcus Rauche[c], Silvia Paasch[c], Konstantin Schutjajew[d,e], Jonas Pampel[d], Friedrich Schwotzer[a], Susanne Dörfler[b], Holger Althues[b], Martin Oschatz[d,e], Eike Brunner[c], Stefan Kaskel[a,b*]

Abstract

For decades graphite has been used as the anode material of choice for lithium batteries since porous carbons were believed to be inappropriate because of their high potential slope during lithiation as well as capacity losses due to intense formation of solid electrolyte interphase (SEI).

However, in this work we demonstrate a microporous carbide-derived carbon material (HCmicro) to provide a high-capacity anode framework for lithium storage in all solid-state batteries. Half-cell measurements of HCmicro exhibit exceptionally high and reversible lithiation capacities of 1000 mAh g^{-1}_{carbon} utilizing an extremely long voltage plateau near 0 V vs. Li/Li^+. The defined microporosity of the HCmicro combined well with the argyrodite-type electrolyte (Li_6PS_5Cl) suppressing extensive SEI formation to deliver high coulombic efficiencies. Preliminary full-cell measurements vs. NMC-cathodes ($LiNi_{0.9}Co_{0.05}Mn_{0.05}O_2$) obtained a considerably improved average potential of 3.76 V leading to a projected energy density as high as 443 Wh kg^{-1}. ^{7}Li Nuclear Magnetic Resonance spectroscopy was combined with ex-situ Small Angle X-ray Scattering and further electrochemical investigations to elucidate the storage mechanism of lithium inside the carbon matrix revealing the formation of extended quasi-metallic lithium clusters.

Introduction

The development of batteries for consumer electronics continually advances volumetric and gravimetric energy density leading to smaller and lighter devices. For electric vehicles, longer range and higher energy density are desired. Lithium metal anodes are attractive candidates to fulfil these goals, owing to their high theoretical specific capacity of 3860 mAh g^{-1} and low voltage of -3.04 V vs. SHE. However, due to the high reactivity of lithium metal causing dendrite formation and electrolyte decomposition, long-term cycling remains problematic under practical conditions.[1–4] Stable negative electrodes like commercial graphite, on the other hand, suffer from low theoretical specific capacity with only little opportunity for further optimization. The ideal anode material therefore combines the high gravimetric capacity of a lithium metal anode with the cycle stability of a graphite anode, gaining long-life batteries with high energy density.

Over the last decades, progress has been made in increasing the lithiation capacity of carbon materials. Several hard carbons (HC) or micro- and mesoporous carbons have been presented exceeding the theoretical capacity of graphite of 372 mAh g^{-1}. Some of them show high specific capacities of 1500 mAh g^{-1} or even beyond in the 1st lithiation.[5–8] However, most of them suffer from limited reversible capacity and usually exhibit a very long so-called sloping region in their voltage profiles, which considerably lowers the resulting full-cell voltage.

Increasing anode capacity at a lower voltage plateau requires the formation of metallic lithium though, which needs to be stabilized for reversible cycling. By adapting the liquid electrolyte and additives or by applying pressure, the long-term stability of lithium-metal batteries could be increased as just recently reported by Dahn et al.[9,10] However, especially at room temperature, plating and stripping of lithium is limited to certain current densities and capacities.[11] When leaving the narrow range of suitable parameters, dendrite formation and porous lithium growth occur as reviewed e.g. by Zhang et al.[4,12] By directing lithium deposition, e.g., using a porous host matrix, a defined interface can be formed that inhibits side reactions with the electrolyte and the effective current density is reduced leading to an enhanced cycle life.[13–17]

A porous carbon material is a good choice as anode material due to its low weight, tunable pore architecture and good electric conductivity. The microporous structure is able to stabilize molecules or metal clusters by decreasing their chemical potential.[18–20] Hence, pores potentially act as seeding sites directing lithium deposition preferentially towards the pore interior. The formation of lithium quasi-metallic clusters – microscopic aggregates consisting of a few tens through a few hundreds of lithium atoms[21] – in the inner porosity of HCs was detected by Tatsumi et al. by ^{7}Li nuclear magnetic resonance (NMR) measurements.[22] Cluster formation is one possibility to store excess lithium at low potentials vs. Li/Li^{+}. Only recently, an operando ^{7}Li NMR study on HC and graphite half-cells has been published by Gotoh et al. investigating overlithiation behavior of the lithium NMR signal in different carbon materials.[23]

We envisioned carbide-derived carbons (CDCs) to offer an ideal microporous carbon framework for stabilizing lithium clusters due to their narrow pore size distribution, which can be precisely tuned.[24–27] However, their high porosity comprises pores that are accessible for small molecules like N_2 or liquid electrolyte components as well as defect sites in the hexagonal carbon structure. In combination with the electronic conductivity of the carbon, both tend to deplete liquid electrolytes and promote solid electrolyte interphase (SEI) formation leading to irreversible lithium and capacity losses.[8,15]

In the following we demonstrate the application of a defined microporous carbide-derived carbon (TiC-CDC,[28] further named as HCmicro) as a carbon/lithium hybrid anode within an all solid-state battery (ASSB) set-up that tackles these challenges and reveals clear advantage compared with a commercial hard carbon (HC). Unlike solvent-based electrolytes, the solid electrolyte cannot penetrate the accessible porosity of the framework, which is why this system suppresses extensive SEI formation

on accessible micropores, and thus, leads to reduced capacity loss in the first cycles as well as long-term stabilization of lithium deposited inside the pores. Half-cell measurements of HCmicro exhibit exceptionally high and reversible lithiation capacities of up to 1000 mAh g^{-1}_{carbon} utilizing an extremely long voltage plateau region near 0 V vs. Li/Li^+. Even at room temperature, no short circuit due to dendrite formation is observed. With the solid electrolyte the herein presented system comprises a remarkably high coulombic efficiency (CE) of 70% in the 1st cycle in comparison with other battery systems utilizing accessible microporous carbon materials, which usually have an initial CE in the range of 30 to 50%.[5,6] Via magic angle spinning (MAS) ^7Li NMR measurements we demonstrate the lithiation mechanism to rely on lithium cluster formation inside the pores with special features for the HCmicro-electrode. The latter, to the best of our knowledge have not been observed for lithiated carbon electrodes so far.[22,23,29–34] Based on these findings, we propose a lithiation mechanism of HCmicro in the all solid-state system via the reversible formation of extended lithium clusters in the carbon framework.

Structural and morphological characteristics of the porous carbon structure

The microporous carbon HCmicro and the commercial HC chosen as reference were initially investigated with regard to their structural and morphological features (Figure 1). Scanning electron microscopy (SEM) and transmission electron microscopy (TEM) revealed the differences of both carbons in terms of carbon nanostructure and particle size. SEM images display particle diameters of around 10 µm for the HC compared to 5 µm for HCmicro while both samples also contain much smaller particles in the range of 1 µm and below. Both carbons show irregular shaped particles with sharp edges. The TEM images depict differences in size and shape of graphite-like domains between HCmicro and HC. These domains show random turbostratic orientation for both carbons with shortened average lateral length of the parallel graphite-like segments for the HCmicro as well as decreased average curvature radius in comparison with the HC. HCmicro additionally comprises a lower average number of parallel stacked graphene sheets overall showing good agreement with literature results for both carbon materials.[35,36]

Nitrogen physisorption analysis at 77 K results in a type I isotherm for HCmicro (Supplementary Figure 1) typical for microporous materials but no accessible porosity for the HC with a type II isotherm characteristic for non-porous materials (according to the IUPAC classification [37]). The specific BET surface area and total pore volume are 1520 $m^2 g^{-1}$ and 0.63 $cm^3 g^{-1}$ for HCmicro and 3.8 $m^2 g^{-1}$ and 0.006 $cm^3 g^{-1}$ for HC, respectively. The pore size distributions of both carbons were determined via quenched-solid density functional theory (QSDFT) calculations (Figure 1c). The main pore diameter in HCmicro is 0.75 nm with 75% of its total pore volume reached at diameters up to 1 nm. Larger micro- and small mesopores until the diameter of 3 nm contribute further. The HC, in comparison, comprises nearly no accessible porosity for N_2 molecules resulting in a very low cumulative pore volume.

As established hard carbons are known to have closed intrinsic porosity, which means pore volume that is present within the material but remains inaccessible in gas physisorption for nitrogen as the probe gas at 77 K. Therefore, we measured Small Angle X-ray Scattering (SAXS) (Figure 1f) to investigate further the porosity of both materials.[38] Both SAXS measurements exhibit scattering curves with comparable intensities at scattering vectors (Q) above 2 nm^{-1} and below 0.3 nm^{-1}. The respective regions are mainly influenced by the scattering of the macroscopic particle surface area for small values of Q and the scattering on micropores for high Q values.[39] In the scattering region between 2 nm^{-1} and 0.3 nm^{-1}, a flattened sloping with higher scattering intensity is observed for HCmicro. According to Saurel et al. pore-pore connections occurring from fractal aggregates of pores lead to an increased contribution of the scattering between Q values corresponding to micropore and particle scattering.[39] This is due to the dimension of the fractal pore-pore connections. Such aggregates can be attributed to an accessible pore structure such as of HCmicro resulting in a higher scattering intensity and flattened slope in this region as observed in the SAXS curves. However, both curves show comparable intensities above 2 nm^{-1} revealing the existence of microporosity for both carbons that differs mainly in inter-pore connectivity.

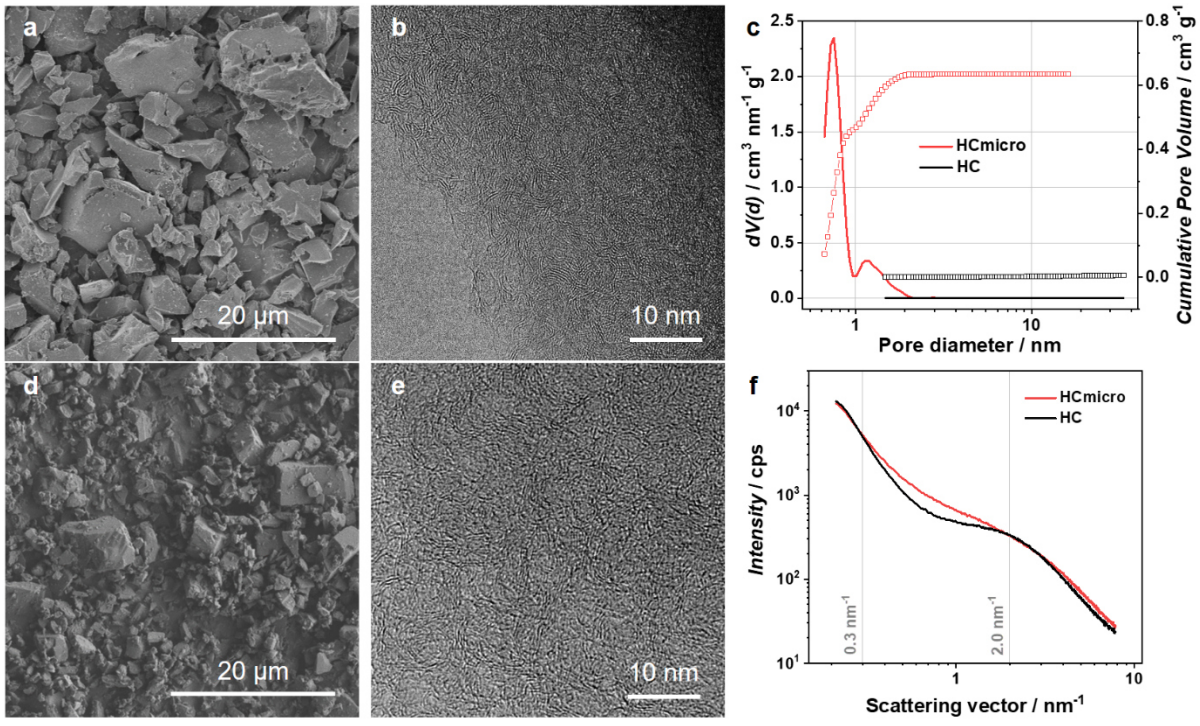

Figure 1: Characterization of the carbon materials. SEM and TEM images of HC (a and b, respectively) and HCmicro (d and e, respectively). Pore size distribution and cumulative pore volume (c) obtained from N_2 physisorption measurements at 77 K (Supplementary Figure 1) and SAXS data (f) for both carbons (red: HCmicro; black: HC).

Further investigations via powder X-Ray Diffraction (PXRD) and Raman measurements are visualized and discussed in the supplementary material (Supplementary Figure 1). In summary, the materials are of comparable morphology and structure with probably slightly lower amount and size of graphite-like

domains for HCmicro. Both carbons possess porosity predominantly in the microporous range, however, with different pore accessibility for N_2 molecules. This leads to the differentiation into "open porous system" for the HCmicro and "closed porous system" for the HC.

Calculation of maximum lithiation capacity for HCmicro

Aurbach et al. proposed a possible lithiation capacity of 1400 mAh g^{-1} for an activated microporous carbon protected against electrolyte penetration by a pyrolytic carbon layer. They calculated the theoretical maximum lithiation capacity based on the complete filling of the microporosity with lithium metal. Practically, however, they have been able to gain only about 10% of this value due to incomplete pore coverage leading to continuous SEI formation during lithium deposition.[15] Our approach therefore employs a solid electrolyte to avoid pore penetration by liquid and supersede any additional carbon coverage e.g. to minimize weight of inactive material.

For calculation of the theoretical maximum of lithium-storage capacity of the herein used HCmicro, we assumed the accessible total pore volume obtained from N_2-physisorption (0.63 $cm^3\ g^{-1}_{HCmicro}$) as accessible void for lithium insertion.[15] Assuming that the density of lithium stored in pores is similar to the bulk density of lithium (0.534 $g_{Li}\ cm^{-3}$), we can estimate the amount of storable lithium in the open pore structure of HCmicro (0.336 $g_{Li}\ g^{-1}_{HCmicro}$ or 1300 mAh g^{-1}). Compared to reversible lithiation capacities of different HCs with a maximum of 550 mAh g^{-1}_{HC} in liquid electrolytes[7] this corresponds to an almost two and a half times higher reversible capacity.

For the definition of the testing parameters, irreversible capacity resulting from side reactions and an incomplete pore filling due to geometric restrictions need to be considered. Hence, for the test protocol in this work, a constant lithiation capacity of 1000 mAh g^{-1}_{carbon} was applied to compare the HCmicro with the commercial HC.

Electrochemical evaluation in half-cells vs. lithium metal

For electrochemical evaluation of the materials in ASSBs, the carbons were prepared as powder electrodes via blending the carbon with solid electrolyte (SE) and a conducting additive in a weight ratio of 60:35:5. The resulting batch powders are denoted as "*active material-electrode*" (graphite-electrode, HC-electrode and HCmicro-electrode) to differentiate from the pure carbon powder. Firstly, the HCmicro-electrode and HC-electrode were evaluated against lithium metal foil. The resulting electrochemical cell is named a "half-cell" due to evaluation of only one electrode (in this case the carbon anode) of the intended battery cell that is then called a "full-cell". All stated potential values in this section are therefore measured vs. Li/Li^+ and shall be read as V or mV "vs. Li/Li^+" though this phrase is not especially written for each individual case. The half-cells were electrochemically evaluated in 10 cycles of lithiation of the carbon anode by discharging with 0.05 mA cm^{-2} up to 1000 mAh g^{-1}_{carbon}

and subsequent charging/delithiation at the same current density until the voltage limit of 2 V was reached (Figure 2).

The resulting voltage profiles for the lithiation of the HCmicro-electrode (Figure 2a) show a short and steep voltage decrease followed by a long plateau below 20 mV. This plateau starts at 172 mAh $g^{-1}_{HCmicro}$ in the 1st cycle and stays above -5.5 mV until the end of lithiation at 1000 mAh g^{-1} for all 10 cycles (see inset). It is noteworthy that the voltage profiles do not comprise a nucleation dip at the beginning of the plateau region. This temporary decrease in cell potential is associated with overcoming the overpotential for the nucleation of lithium metal on a substrates surface and is therefore assigned to the start of lithium metal plating.[23] The delithiation of the HCmicro-electrode exhibits a very long plateau region close to 0 V divided into two parts before the voltage increases sharply at the end of delithiation. During the first delithiation, the first plateau (up to 20 mV) contributes to 210 mAh $g^{-1}_{HCmicro}$ and the second plateau (above 20 mV) adds another 332 mAh $g^{-1}_{HCmicro}$ until the voltage reaches 0.2 V. In total, the plateau capacity reaches 542 mAh $g^{-1}_{HCmicro}$ in the 1st and 827 mAh $g^{-1}_{HCmicro}$ in the 10th cycle. Generally, minor capacity values are obtained in the sloping region above 0.2 V, i.a. due to the nature of the solid electrolyte not being able to form an electrochemical double layer.

The HC-electrode half-cell (Figure 2b) shows a different behaviour in the 1st cycle. The discharge voltage curve falls below -5.5 mV after a capacity of 880 mAh g^{-1}_{HC} and continues to decrease. In further discharge cycles, the cell voltage crosses -5.5 mV shortly after the end of the sloping region forming a slight dip. In the 8th cycle, the voltage signal experiences a sharp rise to 0 V after merely 495 mAh g^{-1}_{HC} of lithiation indicating the formation of a dendrite. Consequently, the cell cannot reach the upper cut-off voltage in the subsequent charging step. However, the 1st charging profile of the HC half-cell still shows a plateau capacity of 338 mAh g^{-1}_{HC} up to 20 mV, corresponding to an increase of ca. 60% when compared to the HCmicro-electrode. The second plateau until 0.2 V exhibits a capacity of 282 mAh g^{-1}_{HC} and is therefore shortened in comparison to the HCmicro-electrode (total plateau capacity of 620 mAh g^{-1}_{HC}).

The two plateaus formed in delithiation of the carbons indicate the existence of two different delithiation mechanisms occurring in both carbons to different extent. The plateau up to 20 mV can be attributed to the stripping of metallic lithium from a 3D structured conducting material due to the small hysteresis between plating and stripping in the case of low current densities (0.05 mA cm^{-2}).[40] The other delithiation plateau between 20 mV and 0.2 V cannot be assigned to a certain species at this point.

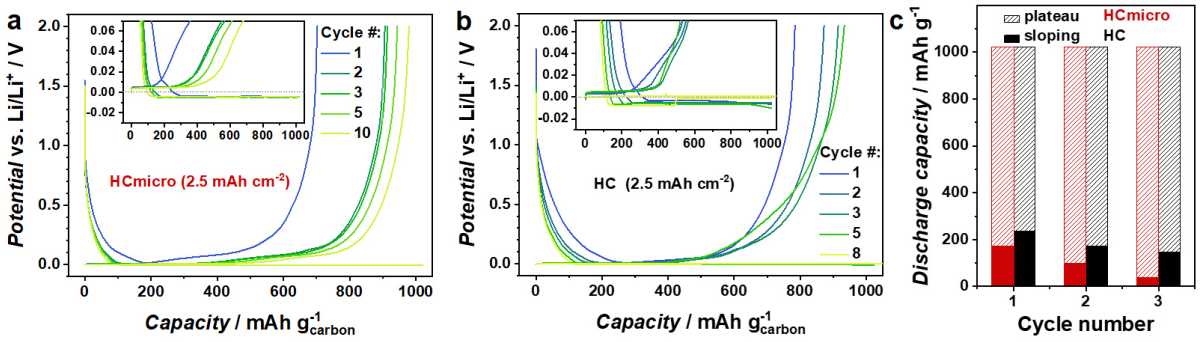

Figure 2: Electrochemical characterization via constant current (CC) measurement. Voltage profiles of HCmicro (a) and HC (b) half-cells vs. lithium metal galvanostatically cycled at 0.05 mA cm^{-2} between 2 V and a constant capacity of 1000 mAh g^{-1}_{carbon} in discharge with an areal loading of 2.5 mAh cm^{-2}. (c) Comparison of sloping (until 20 mV, filled area) and plateau discharge capacities (below 20 mV, hatched area) for both carbon half-cells in the first 3 cycles.

The HCmicro half-cell reaches slightly lower initial CE (70%) than the HC half-cell (77%) but improves rapidly to 98% CE with a delithiation capacity of 980 mAh $g^{-1}_{HCmicro}$ in the 10th cycle. In contrast, the HC half-cell fails in 8th lithiation due to micro short-circuit of the cell. The shown example for a HC half-cell, however, is no outlier. We tested various HC half-cells each failing due to short-circuit within their first 8 cycles while HCmicro half-cells did not show this phenomenon. Despite the fact that no liquid electrolyte penetrates the pores, the lower initial CE is not unusual for a porous carbon with a high specific surface area, since, e.g., lithium can react with carbon dangling bonds at the carbon surface. In the following cycles, the CE for HCmicro half-cell show remarkably high values compared to other carbon electrodes with N_2-accessible porosity stated in literature.[5,6,41] The application of HCmicro in liquid electrolyte systems cannot compete with the herein stated all solid-state system in terms of CEs and delithiation capacities.[8,28] This indicates that the combination of the open porous HCmicro with the solid electrolyte prevents penetration of electrolyte components into the microporous system and thus minimizes side reactions with lithium species located inside the carbon particle.

As the constant current (CC) experiments exhibit a high capacity slightly below 0 V in the plateau region, we assumed a thermodynamically favoured formation of lithium species inside the carbon. Hence, we conducted a constant voltage measurement (ConVol) in which the half-cells were lithiated until 0 V, and subsequently a constant voltage of 0 V was applied until the current exceeds -7.5 µA cm^{-2} (Figure 3). According to our understanding, bulk lithium metal should not deposit under these conditions since a certain overvoltage is normally required for plating. The resulting voltage profiles show a sloping region and continue with a plateau at the cut-off voltage of 0 V during discharge. The sloping and plateau capacities were separated at a potential of 20 mV to examine the differences between HC- and HCmicro-electrode (Figure 3c). The obtained capacities of the sloping region are quite comparable with slightly higher values close to 150 mAh g^{-1}_{HC} for the HC half-cell. However, the plateau capacities show a

remarkable difference with values of 108 to 92 mAh g^{-1}_{HC} for HC and 457 to 330 mAh $g^{-1}_{HCmicro}$ for HCmicro half-cells. As the plateau capacity at 0 V in the delithiation of HCs was assigned to lithium insertion into microporous structure by Stevens and Dahn,[42] we can presume that our measured capacity for the HCmicro-electrode results from lithium species forming inside the micropores. There are two possible lithium species known from literature forming at potentials near and slightly below 0 V – lithium clusters and lithium metal.[23,31]

For the interpretation of the ConVol measurements, it is important to state that the minimum potential of the cell in constant voltage step was at -0.5 mV slightly below the intended 0 V due to the precision of the measurement device. However, this is at least one order of magnitude smaller than the overpotential for lithium metal plating observed in CC experiments e.g. for Li-Ni-foil cell and Li-Li symmetric cell (Supplementary Figure 2). Therein the minimum of the potential dip attributed to the beginning of lithium metal plating was located at values of -64.0 mV and -5.0 mV, respectively. Additionally, the delithiation profile of the cells has only one plateau region at potentials between 0.02 and 0.2 V corresponding to the higher potential plateau in CC measurements. The first plateau below 0.02 V, previously assigned to the stripping of lithium metal, is missing. This suggests that no lithium metal plating occurs in these experiments. In contrast, it shows the high capacity-gain by another lithium form different from sloping capacity or formation of graphite intercalation compounds (GICs) like LiC_6 (both above 0 V), and higher than cluster formation in hard carbons. In the 3rd charging cycle the HCmicro cell exhibits a short circuit due to dendrite formation caused by the lithium metal counter electrode. However, this has no influence on its previous performance and can be easily prevented by using less dendrite-prone counter electrodes than lithium metal, e.g., a lithium-indium alloy. The conducted cyclovoltammetry (CV) measurements on the HCmicro half-cell (see Supplementary Figure 3) confirm that no plating of lithium metal occurs at potentials above and at -5 mV as they do not comprise the classical plating/stripping peaks as visible in Li-Ni-foil cell cyclovoltammetry (Supplementary Figure 3) or shown by Bonino et al. [43].

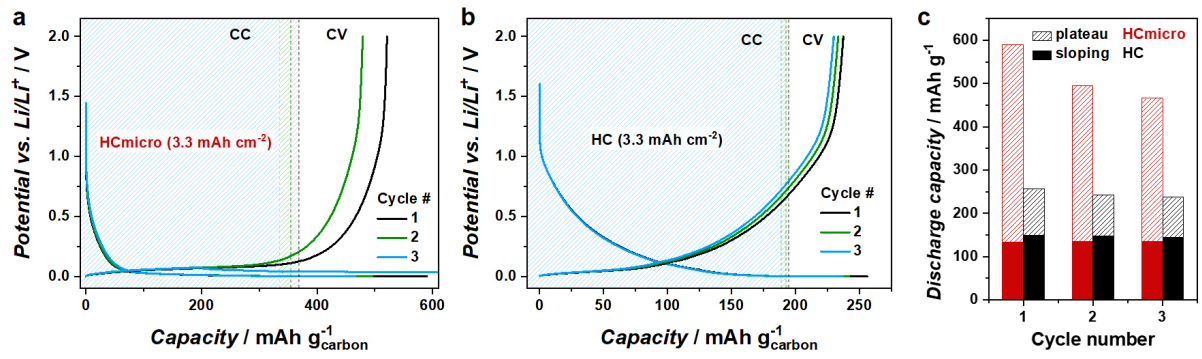

Figure 3: Electrochemical characterization via constant voltage (ConVol) measurement. Galvanostatic measurements including a constant voltage step at 0 V during discharge until a cut-off current of -7.5 µA cm^{-2} for HCmicro (a) and HC (b) half-cells vs. lithium metal with constant current (CC, hatched area) and constant voltage (CV) regions of the discharge/lithiation voltage profiles

separated by dotted lines in (a) and (b). (c) The corresponding capacities for sloping (until 20 mV, filled area) and plateau (below 20 mV, hatched area) region gathered from the discharge voltage profiles for HC (black) and HCmicro (red).

In summary, the carbide derived carbon anode material (HCmicro) exhibits major advantages in half-cell performance comprising plateau capacity near 0 V vs. Li/Li^+, high CE and delithiation capacity. HCmicro did not undergo any short-circuiting despite the fact that a high loading of 2.5 mAh cm^{-2} was cycled and the measurements were performed at room temperature. To fully understand and explain the mechanism for this high plateau capacity, further investigations were conducted via NMR spectroscopy and SAXS measurements.

^{7}Li NMR spectroscopy studies of lithiated electrode materials

Magic angle spinning ^{7}Li nuclear magnetic resonance (^{7}Li MAS NMR) spectra were measured ex-situ for varying stages of lithiation of graphite-, HC- and HCmicro-electrode to obtain further information about the evolving lithium structures and lithiation mechanism in the described cell system (Figure 4). Therefore, half-cells comprising the particular batch powders were pre-cycled once between 0.01 and 2 V and afterwards discharged (lithiation of active material) until a certain cut-off criterion. The chosen cut-off criteria were defined as 10 mV (stage 1), the typical lithium intercalation cut-off for graphite anodes, and 750 mAh g^{-1}_{carbon} (stage 2), for investigation of lithium species at highly lithiated stage (Figure 4a). To investigate the influence of lithium contained in the SE, the NMR spectrum was also measured on the pristine HCmicro-electrode. The resulting spectrum (Figure 4c) displays one intense signal at 1 ppm with spinning side bands of first and second order marked with asterisks (*) in the diagram. Signals with very low chemical shift against the reference LiCl arise from ionic lithium species. Hence, the signal is attributed to lithium in the Li_6PS_5Cl argyrodite-type electrolyte.[19,31]

The graphite-electrode material cycled to stage 1 (10 mV) was investigated to gain information about the solid-state ^{7}Li MAS NMR signal of intercalated lithium. In addition to the electrolyte signal at 1 ppm, the spectrum exhibits a peak at 48 ppm as expected from literature revealing full lithiation to the graphite intercalation compound (GIC) stage I (LiC_6).[44–46]
The HCmicro-electrode lithiated until 10 mV did not develop any signal apart from the electrolyte signal, which becomes slightly broadened compared with the pristine HCmicro-electrode. GICs with lower lithium content like diluted stages III and IV[46] are located at low chemical shift in NMR and therefore might overlap with the intense solid electrolyte peak at 1 ppm.[45,47] The formation of GIC stage I (LiC_6) in HCmicro is unlikely due to the low density of perfect graphitic domains observed in TEM (see Figure 1). This explains the absence of the NMR peak at 48 ppm.

At 750 mAh g^{-1}_{HC} lithiation (stage 2) of the HC-electrode a very broad signal starting from approximately 35 ppm with its maximum at 105 ppm and almost reaching the first spinning side band of the electrolyte peak at 130 ppm occurs (Figure 4b and c). Besides the electrolyte peak also another signal at 263 ppm was observed. This signal can be assigned to metallic lithium deposited in the electrode powder according to literature.[23,34,48] The broad signal around 105 ppm falls into the range between intercalation signals from 0-50 ppm and the lithium metal at 263 ppm. According to literature we therefore assign it to lithium clusters in the HC material.[23,32,34,44,49]

The HCmicro-electrode lithiated to stage 2 (750 mAh $g^{-1}_{HCmicro}$) exhibits a distinct broad signal centered at 175 ppm chemical shift. Further the signal at 263 ppm beforehand assigned to formation of lithium metal in the electrode powder occurs in addition to the electrolyte peak at 1 ppm. The metallic lithium signal is less intense for the HCmicro-electrode at stage 2 compared to the signal in the HC-electrode (Figure 4b). This hints to a smaller amount of lithium metal in the HCmicro-electrode as the integral in NMR corresponds to the number of associated nuclei at comparable sample weight. The short-circuit observed in electrochemical cycling of the HC half-cells in contrast to the HCmicro half-cells supports this observation (Figure 2b). The signal of the HCmicro-electrode at 175 ppm could not be assigned to any chemical shift in room temperature ^{7}Li NMR spectra for disordered carbon electrodes known from literature.[23,32,34,49] However, it also falls into the range of chemical shift predicted for lithium clusters between 50 and 263 ppm.[44]

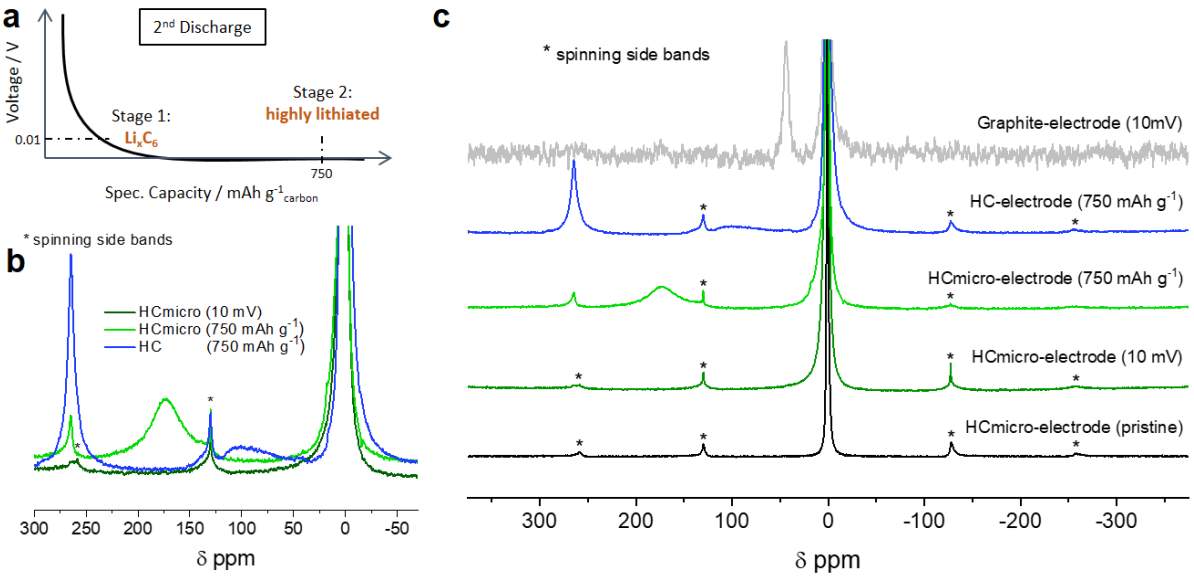

Figure 4: ^{7}Li NMR spectroscopy at different lithiation degree. Schematic voltage profile of the half-cells in preparation for NMR measurement displaying second discharge with different cut-off stages for cell disassembly (a). Room-temperature ^{7}Li MAS NMR spectra are shown with enlarged spectra of HCmicro-electrode at stages 1 and 2 and HC-electrode at stage 2 for detailed signal comparison (b). The full spectra of the different samples as described above are provided in (c). Spinning side bands are denoted by asterisks (*).

A number of research groups have studied lithium cluster formation in HCs in combination with liquid electrolytes observing ^{7}Li NMR signals at chemical shifts between 50 ppm and 120 ppm at room temperature.[23,32,34,49] The relatively high chemical shift of 175 ppm observed for the lithiated HCmicro-electrode is therefore rather unusual compared to literature-known HC cluster-signals and the herein described HC-electrode measurements. There are two different possibilities to explain the observed phenomenon. The first one is a higher free electron content in the clusters, which results in a Knight shift of the signal due to deshielding of the lithium nuclei.[44] This can occur due to a larger cluster size and would lead to a higher chemical shift of the ^{7}Li NMR signal. In terms of conductivity, increasingly large clusters become more and more metallic. This results in effective chemical shifts closer to the signal of lithium metal than to the GIC peak.[44] The second possible explanation originates from the low graphitic structure of HCmicro. According to Tatsumi et al., the chemical shift of lithium clusters formed in HC is determined by the chemical exchange between clusters in microcavities and GICs. It is consequently moved to lower chemical shifts at room temperature while it splits into two peaks at -30 °C.[22,33,34] The cluster signal for HC pore filling at temperatures below -30 °C can be found at a chemical shift of approximately 180 ppm, which is in good agreement with the chemical shift of the herein depicted ^{7}Li NMR signal at room temperature. Lithiated HCmicro might lack this shift due to the minor content of ordered graphite domains, which was pointed out earlier by TEM measurements. Further low temperature NMR measurements are required at this point to undoubtedly explain the observed signal. However, it can be concluded that lithium clusters exist in the lithiated HCmicro material, and that the lithium formation inside the HCmicro-electrode differs from the configuration in HCs.

Small Angle X-ray Scattering (SAXS) of lithiated HCmicro

Further investigation on the HCmicro-electrode powder via SAXS measurement in sealed capillaries revealed a change of the scattering profile before and after lithiation (Figure 5). Therefore, the HCmicro-electrode was measured in the pristine and the lithiated stage discharged until 750 mAh $g^{-1}_{HCmicro}$ after pre-cycling with one initial formation cycle between 0.01 and 2 V. The obtained scattering profiles show a lowered intensity between 1 and 8 nm^{-1} scattering vector for the lithiated HCmicro-electrode, which implies lower contribution of the scattering of single and aggregated micropores to the overall scattering. The difference in scattering intensity is also confirmed by measurements at various spots of the samples revealing identical scattering. This indicates a loss in microporosity due to lithium insertion inside the pores. A corresponding insertion mechanism has been described by Stevens et al. for lithium insertion in hard carbon material.[42]

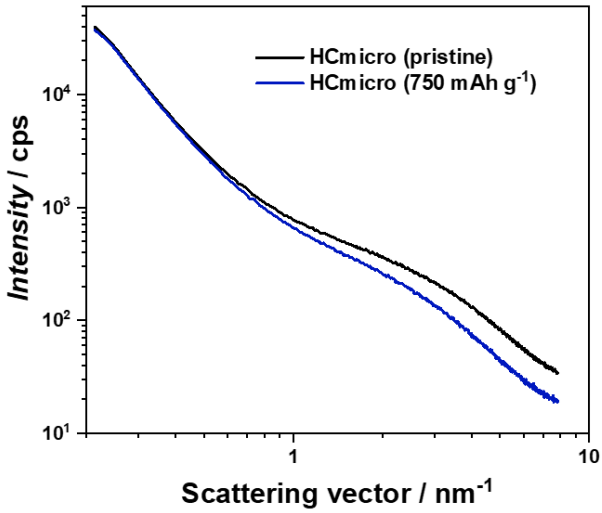

Figure 5: SAXS analysis of HCmicro. SAXS profiles of pristine (black) and lithiated HCmicro-electrode (blue) after pre-cycling in a half-cell vs. lithium metal between 0.01 and 2 V with a lithiation capacity of 750 mAh $g^{-1}_{HCmicro}$.

Based on these findings we can assume that the lithium gathers inside the microporosity of the HCmicro during electrochemical lithiation. We therefore propose a unique lithiation mechanism for HCmicro in all solid-state batteries as follows (Figure 6).

Proposal for lithium insertion mechanism

The second plateau observed in the delithiation step of both carbons in the constant current and the constant voltage experiments is a unique observation for the HCmicro, which shows no plateau capacity in liquid-electrolyte experiments.[8,50] A theoretical study on a graphene hetero structure with large interlayer distance by Bijoy and Murugan predicted the stabilization of extended lithium clusters between the layers with a slightly expanded interlayer distance of 3.4 Å.[51] In combination with our studies, this suggests the existence of such lithium clusters stabilized between the pore walls of HCmicro. The spatial pore-pore connection in HCmicro furthermore leads to connected pore voids and enables the formation of extended lithium clusters and advanced lithium storage compared to HC although comparable results concerning the size of micropores for both carbons were obtained in SAXS measurements. In larger pores, more clusters can combine. Thereby, they also eventually gain characteristics of bulk lithium, which is suggested by the existence of a short linear plateau at the beginning of the delithiation step and by the bulk lithium signal in ^{7}Li NMR despite the missing of a typical plating dip in the voltage profiles of the HCmicro.

Hence, we assign the second plateau of the electrochemical investigation of the half-cells to the delithiation of lithium clusters inside the porosity of the carbons. The higher capacity reached in this region for HCmicro-electrode compared to the HC-electrode gives further evidence for a higher amount of lithium nuclei assembled in its cluster structures as concluded from ^{7}Li MAS NMR measurements. Consequently, we propose that the formation of extended lithium clusters in the pore-pore connected,

accessible microporous system of the HCmicro is facilitated by the combination with the herein employed solid-state electrolyte.

In summary, the following mechanism for lithium insertion into HCmicro in an all solid-state set-up is proposed (Figure 6). As established in literature for hard carbons, the lithium ions firstly adsorb on defects or edges of the carbon surface in the sloping region of the potential curve. In the following potential plateau intercalation of Li^+ in the small graphite-like domains of the HCmicro takes place.[52] Subsequently, lithium ions deposited at the edge of graphite-like domains and on pore walls start to form clusters which will extend in size upon further lithiation.[24,53] At a certain point, the growth of lithium metal will take place either when cluster size reaches high numbers of nuclei resulting in rearrangement, or eventually, the lithium may even start plating on the outer shell of the carbon when the porosity is completely filled. However, lithium metal formation occurs very homogeneous and no short-circuits were observed for HCmicro-electrode since there is a smooth transition from cluster to bulk lithium. We therefore name the herein presented approach a carbon/lithium hybrid anode-concept.

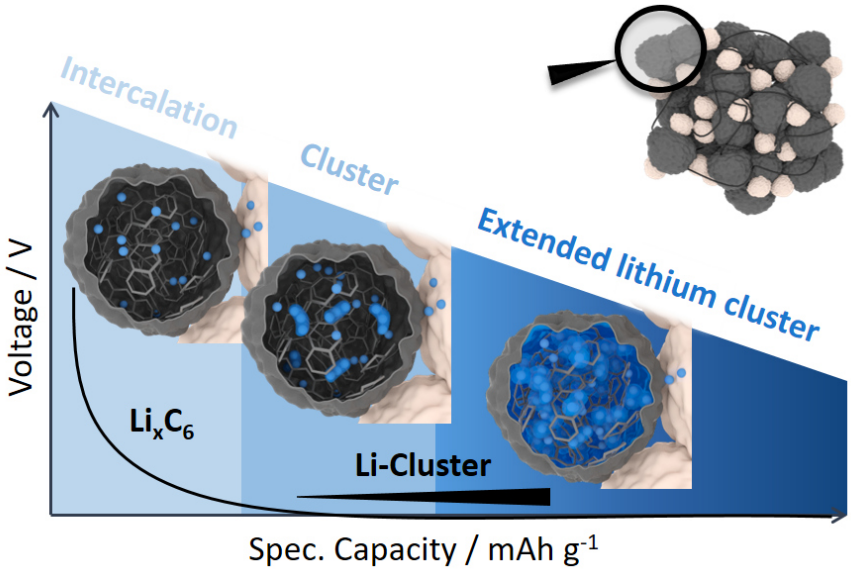

Figure 6: Proposed mechanism of lithium insertion in microporous carbon as anode material in all solid-state batteries. Scheme divided into 3 phases: the intercalation of lithium, cluster formation as known from hard carbon lithiation and the formation of extended lithium clusters as special feature of the HCmicro anode material in all-solid-state electrolyte.

Stable full-cell performance vs. NMC cathode

The excellent performance of the half-cells motivated us to demonstrate the first full-cell results combining the described carbon anode concept with a suitable cathode material (Figure 7 and Supplementary Figure 4). The full-cells consisting of a HCmicro-electrode anode and a nickel-rich NMC ($LiNi_{0.9}Mn_{0.05}Co_{0.05}O_2$) cathode with Li_6PS_5Cl electrolyte exhibit relatively stable reversible

cycling performance over 40 cycles with coulombic efficiencies exceeding 98% in 10th cycle and at least 75% initial CE. The capacity of the cells starts with 174 mAh g$^{-1}_{NMC}$ concluding with 92 mAh g$^{-1}_{NMC}$ in 40th cycle. Based on the weight of the anode active material, this capacity results in 625 mAh g$^{-1}_{HCmicro}$ for the 1st cycle. The average voltage was calculated via the measured energy and capacity values of specific cycle step of the cell with 3.76 V in first discharge improving to 3.79 V in 10th cycle and continuing at this value until 40th cycle (see Supplementary Note 1). This is a clear improvement compared to the average voltage of 3.55 V in first discharge for a HC-electrode full-cell with comparable composition continued with 3.53 V for 3rd discharge (see Supplementary Figure 4). It should be mentioned that these results are the very first experiments on highly microporous carbons with reversible capacity as high as 1000 mAh g$^{-1}_{carbon}$ in combination with argyrodite-type solid electrolyte and with a nickel-rich cathode. Especially, these electrodes were assembled without any pre-lithiation of the carbon anode or other additional lithium content. Therefore, all of the lithium capacity derives from the dry film NMC cathode[54] and there is no additional lithium to replace irreversibly reacted lithium from side reactions in the first cycles. As a consequence, these results underline the reversible (de)lithiation concept of the HCmicro anode. So far, no further optimization was conducted regarding the balancing of electrodes, the particle size and shape of the carbon or other commonly used procedures for commercial battery improvement. Consequently, these results are of high value and are expected to be further improved, e.g., by pre-lithiation of the carbon via chemical or physical approaches.[55,56] Theoretical calculation of the investigated ASSB cell revealed projected gravimetric and volumetric energy densities of 443 Wh kg^{-1} and 1001 Wh L^{-1} for the complete cell stack at n/p = 1 as utilized in the experiment assuming an SE layer thickness of 30 µm (detailed calculation see Supplementary Table 1 and 2 plus Notes).

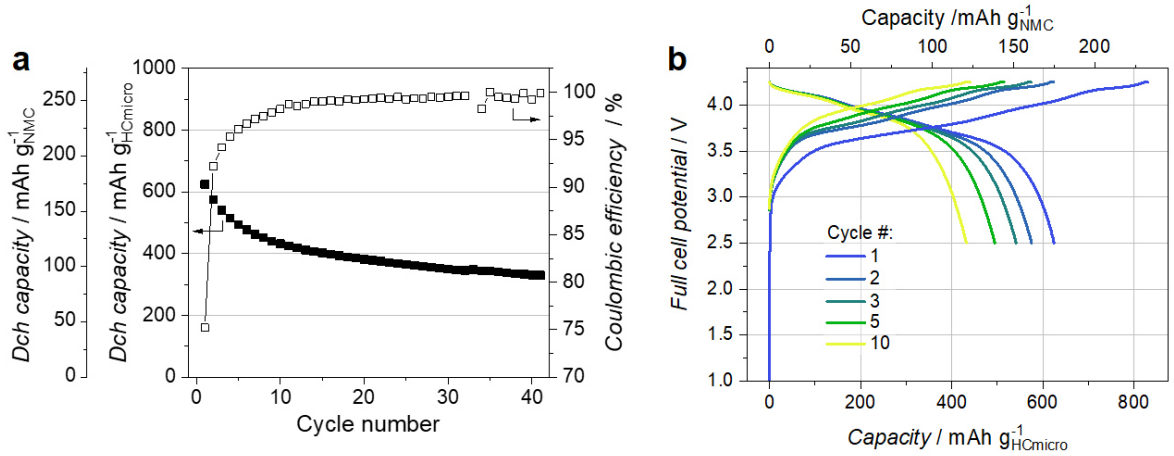

Figure 7: Electrochemical characterization in full-cells. Discharge (Dch) capacities calculated based on HCmicro (anode) and NMC content (cathode) and coulombic efficiency of HCmicro/NMC all solid-state full-cell (a) as well as voltage profiles of the first cycles shown in capacity per NMC (upper axis) and per HCmicro (lower axis) (b).

Conclusion

Summarizing our findings, we were able to show a carbon/lithium hybrid anode-concept based on the microporous carbon anode material TiC-CDC (HCmicro) in an all solid-state battery to obtain high and, above all, reversible lithiation capacities of 1000 mAh $g^{-1}_{HCmicro}$ with initial CE as high as 70% in half-cells.

The advancement regarding the cell concept presented herein is the long plateau region in the potential profile of the half-cell measurements at very low potential vs. Li/Li^+, which is a desired characteristic in order to significantly enhance full-cell energy density. Our investigations of the lithiation mechanism revealed the formation of lithium clusters inside the open pore system of HCmicro by ^7Li MAS NMR cluster signal and gave evidence for a distinct lithium formation mechanism compared to hard carbon lithium clusters indicated by the characteristic chemical shift of the formed species. The unique combination of a porous carbon with the solid electrolyte enables the storage of highly dispersed and stabilized quasi-metallic lithium, which results in a highly reversible cell performance at room temperature. Finally, such a hybrid lithium-HCmicro anode concept was successfully combined and cycled 40 times vs. a nickel-rich NMC cathode. Without any extra lithium source beside the NMC cathode material, these full-cells obtained 174 mAh g^{-1}_{NMC} in 1st discharge and more than half of the initial capacity remained in 40th cycle. The average full-cell potential improved significantly compared with the HC full-cell by more than 0.2 V to a value of 3.76 V for the HCmicro full-cell, which leads to a projected energy density as high as 443 Wh kg^{-1}.

This work demonstrates the potential of porous carbons as 3-dimensional framework architectures for the stabilization of metallic or cluster-type lithium. The possibility to tune pore size, pore volume and pore functionalization of carbon materials and their combination with solid electrolytes is a promising option for the production of high capacity anodes for future high energy density prototype cells.

Methods

Materials

The carbon materials used for electrode preparation – hard carbon (HC, Kuraray Co., Ltd.), carbide-derived carbon (TiC-CDC-1000, HCmicro) and graphite powder – were dried for 12 h at 200 °C under vacuum before use. The TiC-CDC-1000 (HCmicro) was synthesized at Technical University Dresden from TiC particles (Sigma Aldrich, -325 mesh, 98%) via chlorination process at 1000 °C as previously described by Borchardt et al. [57] Argyrodite type solid electrolyte (Li_6PS_5Cl, SE) with approx. 3 µm and 15 µm particle diameter was utilized as received for electrode batch preparation and SE pellet in cell stacks, respectively. Lithium metal foil was purchased with a thickness of 50 µm from China Energy Lithium Co., Ltd. and was prepared in an Ar-filled glove box via punching out disks with 13 mm diameter. Li_2O-ZrO_2 (LZO) coated $LiNi_{0.9}Co_{0.05}Mn_{0.05}O_2$ (NMC) was prepared by the sol-gel method based on ZrO_2 coating as stated in a previous publication.[54]

All further material handling and cell preparation was conducted under inert gas atmosphere in an Ar-filled glovebox with moisture and air content below 0.01 ppm.

Electrode materials preparation

To prepare the anode composite electrode powders further named as HCmicro-, HC- and graphite-electrode, the dried carbon - HCmicro, HC and graphite, respectively - was mixed manually with conductive carbon additive (CNF, CNF_PR-25-XT-HHT, Pyrograf), and SE (Li_6PS_5Cl, 3 µm particle diameter) in the mass ratio of 60:5:35 for 30 min in an agate mortar.

NMC-cathodes for full-cell experiments were prepared via dry-film processing as described by Hippauf et al. [54] with 16.1 mg_{AM}/cm^2 loading of LZO-coated NMC with a mass ratio of 85:2:13 of NMC:CNF:SE.

Half-cell and full-cell preparation

The half-cells were prepared in a stainless steel outer casing with a polyoxymethylene liner by using a die with a diameter of 13 mm. Therefore, a lithium foil with a diameter of 13 mm and 50 µm thickness was arranged inside the die and SE powder (150 mg ±0.5 mg) was uniformly spread on top by a micro-spatula. This composition was temporarily compressed and compacted into a pellet. Afterwards, the composite powder HCmicro-, HC- or graphite-electrode, respectively, (7.37 mg ±0.2 mg) was homogeneously distributed across the compacted electrolyte surface in the die and again compressed by using a hydraulic press applying 4 tons for 30 s. The resulting areal active material loading of the half-cell was 3.33 mg cm^{-2}. Before cell performance measurement, the cells were closed airtight inside a pouch bag.

Full cells were prepared similar to half-cell preparation except for the lithium foil, which was replaced by the NMC-cathode and was positioned centered on top of the SE pellet after the carbon-anode preparation and the SE pellet formation.

Electrochemical measurements

All cells were stored for 5 hours after assembly before electrochemical measurement started. The cell performance measurements were conducted on a battery tester CTS-Lab (BaSyTec, Germany). The half-cells were discharged with 0.05 mA cm^{-2} until a constant capacity of 1000 mAh g^{-1} or cut off if going below -0.02 V earlier followed by a 30-min-pause and a subsequent charging at the same areal current density until 2 V. This procedure was repeated for 10 cycles.

The full-cells were cycled between 2.5 and 4.25 V with a constant voltage step at the end of each charging until a cut-off current of 0.015 mA cm^{-2}. The areal current density was 0.05 mA cm^{-2} as well.

Further electrochemical experiments were conducted on a VSP-300 (Bio-Logic, France). Constant voltage measurements (ConVol) were conducted with pre-cycling between 0.01 and 2 V with a current density of 0.05 mA cm^{-2} for 2 times. A constant current (CC) step in discharge with 0.05 mA cm^{-2} until

0 V and subsequent ConVol step at 0 V until a cut-off current of -7.5 µA cm^{-2} followed for 3 cycles with in between charging at 0.05 mA cm^{-2} to 2 V.

Cyclovoltammetry (CV) procedure was conducted with 0.01 mV s^{-1} between the upper cut-off voltage at 1 V and changing lower cut-off voltages of 10, 2, 0 and -5 mV each for 4 cycles. The I-step duration was set to 50%.

Materials characterization

Powder X-ray diffraction (XRD) patterns were measured on a Bruker D8 in Bragg-Brentano geometry in a 2Θ range of 10-70 ° with a resolution of 0.03 ° using CuKα radiation (λ=0.15418 nm) and a NaI scintillation detector. The samples were placed on a horizontal silicon single crystal holder.

Nitrogen physisorption isotherms were measured via low-pressure nitrogen physisorption at 77 K with an Autosorb 1C apparatus (Quantachrome), using 10-20 mg of activated sample. Activation was conducted under vacuum for 12 h at 200 °C after a heating period of 2 h on a Belprep Vac II. The multipoint BET equation (p/p_0 = 0.05-0.2) served for calculation of the specific surface area, whereas pore volumes were estimated from the volume of adsorbed nitrogen at p/p_0 = 0.97 for the micro- and mesoporous content. The quenched-solid density functional theory (QSDFT) for nitrogen at 77 K on carbon with slit/cylindrical pores (adsorption branch) was utilized to retrieve the pore size distributions (PSDs).

For Raman measurements, a Renishaw inVia microscope with an excitation laser wavelength of 514 nm at 5% laser power (0.1 mW $µm^{-3}$) and 50-fold magnification was used measuring between 100 and 3500 cm^{-1} for two times 30 s. The intensity ratio I(D)/I(G) was calculated from the fitting of G-Peak via Breit-Wigner-Fano and D-Peak with Lorentz fitting with a linear base line analysed from 1200 cm^{-1} to 1750 cm^{-1}.

Small-angle X-ray scattering was measured on a Bruker Nanostar 2 device using $Cu_{Kα}$ radiation in transmission geometry with 279 mm distance between sample and detector at a vacuum level of approximately 0.02 mbar. Prior to each measurement, samples were filled into borosilicate capillaries inside the glovebox, temporarily closed with polymer foil and finally sealed by melting the glass, immediately after extraction from the glovebox.

Solid-state ^{7}Li MAS NMR experiments were carried out on a BRUKER Avance NEO 300 MHz spectrometer at a resonance frequency of 116.6 MHz with a commercial double resonance 2.5 MAS NMR probe operating at a MAS frequency of 15 kHz. 32 Scans were accumulated. The pulse repetition time was 60 s. SPINAL 1H-decoupling was applied during signal acquisition. The lithium chemical shift was referenced with LiCl.

The TEM investigations were conducted using a double-Cs-corrected Jeol ARM200F, equipped with a cold field emission gun and operated with an acceleration voltage of 80 kV as well as on a TEM JEM-211, JEOL.

Scanning electron microscopy (SEM) was performed on a HITACHI SU8020 at 2.0 kV with a working distance of 8.9 and 15.3 mm for HC and HCmicro, respectively. The samples were sputtered on a Q150R ES (Quorum) with Au nanoparticles (≤ 10 nm) before SEM measurement.

References

1. Wu, F., Maier, J. & Yu, Y. Guidelines and trends for next-generation rechargeable lithium and lithium-ion batteries. *Chemical Society reviews* **49,** 1569–1614; 10.1039/C7CS00863E (2020).
2. Lin, D., Liu, Y. & Cui, Y. Reviving the lithium metal anode for high-energy batteries. *Nature nanotechnology* **12,** 194–206; 10.1038/NNANO.2017.16 (2017).
3. Li, L., Li, S. & Lu, Y. Suppression of dendritic lithium growth in lithium metal-based batteries. *Chemical communications* **54,** 6648–6661; 10.1039/c8cc02280a (2018).
4. Cheng, X.-B., Zhang, R., Zhao, C.-Z. & Zhang, Q. Toward Safe Lithium Metal Anode in Rechargeable Batteries: A Review. *Chemical reviews* **117,** 10403–10473; 10.1021/acs.chemrev.7b00115 (2017).
5. Xu, B. *et al.* Nano-CaCO3 templated mesoporous carbon as anode material for Li-ion batteries. *Electrochimica Acta* **56,** 6464–6468; 10.1016/j.electacta.2011.04.130 (2011).
6. Velez, V. *et al.* Synthesis of novel hard mesoporous carbons and their applications as anodes for Li and Na ion batteries. *Carbon* **147,** 214–226; 10.1016/j.carbon.2019.02.083 (2019).
7. Kubota, K. *et al.* Structural Analysis of Sucrose-Derived Hard Carbon and Correlation with the Electrochemical Properties for Lithium, Sodium, and Potassium Insertion. *Chem. Mater.*; 10.1021/acs.chemmater.9b05235 (2020).
8. Sakamoto, K. M. Master`s Thesis. Naval Postgraduate School, 2011/09.
9. Weber, R. *et al.* Long cycle life and dendrite-free lithium morphology in anode-free lithium pouch cells enabled by a dual-salt liquid electrolyte. *Nat Energy* **4,** 683–689; 10.1038/s41560-019-0428-9 (2019).
10. Louli, A. J. *et al.* Exploring the Impact of Mechanical Pressure on the Performance of Anode-Free Lithium Metal Cells. *J. Electrochem. Soc.* **166,** A1291-A1299; 10.1149/2.0091908jes (2019).
11. Bai, P., Li, J., Brushett, F. R. & Bazant, M. Z. Transition of lithium growth mechanisms in liquid electrolytes. *Energy Environ. Sci.* **9,** 3221–3229; 10.1039/C6EE01674J (2016).
12. Cheng, X.-B. *et al.* A Review of Solid Electrolyte Interphases on Lithium Metal Anode. *Advanced science (Weinheim, Baden-Wurttemberg, Germany)* **3,** 1500213; 10.1002/advs.201500213 (2016).
13. Zhao, C.-Z. *et al.* Designing solid-state interfaces on lithium-metal anodes: a review. *Sci. China Chem.* **62,** 1286–1299; 10.1007/s11426-019-9519-9 (2019).
14. Shi, P. *et al.* A Review of Composite Lithium Metal Anode for Practical Applications. *Adv. Mater. Technol.* **5,** 1900806; 10.1002/admt.201900806 (2020).

15. Isaev, I. *et al.* A new approach for the preparation of anodes for Li-ion batteries based on activated hard carbon cloth with pore design. *Journal of Power Sources* **119-121,** 28–33; 10.1016/S0378-7753(03)00119-8 (2003).
16. Ye, W. *et al.* Stable Nano-Encapsulation of Lithium Through Seed-Free Selective Deposition for High-Performance Li Battery Anodes. *Adv. Energy Mater.* **10,** 1902956; 10.1002/aenm.201902956 (2020).
17. Zheng, G. *et al.* Interconnected hollow carbon nanospheres for stable lithium metal anodes. *Nature nanotechnology* **9,** 618–623; 10.1038/NNANO.2014.152 (2014).
18. Hippauf, F. *et al.* The Importance of Pore Size and Surface Polarity for Polysulfide Adsorption in Lithium Sulfur Batteries. *Adv. Mater. Interfaces* **3,** 1600508; 10.1002/admi.201600508 (2016).
19. Oschatz, M. *et al.* (Elsevier2016), pp. 237–318.
20. Seitz, A. E., Hippauf, F., Kremer, W., Kaskel, S. & Scheer, M. Facile storage and release of white phosphorus and yellow arsenic. *Nature Communications* **9,** 361; 10.1038/s41467-017-02735-2 (2018).
21. Sugano, S., Nishina, Y. & Ohnishi, S. *Microclusters. Proceedings of the First NEC Symposium, Hakone and Kawasaki, Japan, October 20-23, 1986* (Springer, Berlin, Heidelberg, 1987).
22. Tatsumi, K. *et al.* 7Li NMR studies on a lithiated non-graphitizable carbon fibre at low temperatures. *Chem. Commun.,* 687–688; 10.1039/A700221A (1997).
23. Gotoh, K. *et al.* Mechanisms for overcharging of carbon electrodes in lithium-ion/sodium-ion batteries analysed by operando solid-state NMR. *J. Mater. Chem. A* **8,** 14472–14481; 10.1039/D0TA04005C (2020).
24. Morita, R. *et al.* Combination of solid state NMR and DFT calculation to elucidate the state of sodium in hard carbon electrodes. *J. Mater. Chem. A* **4,** 13183–13193; 10.1039/c6ta04273b (2016).
25. Gogotsi, Y. *et al.* Nanoporous carbide-derived carbon with tunable pore size. *Nature Materials* **2,** 591–594; 10.1038/nmat957 (2003).
26. Chmiola, J., Yushin, G., Dash, R. & Gogotsi, Y. Effect of pore size and surface area of carbide derived carbons on specific capacitance. *Journal of Power Sources* **158,** 765–772; 10.1016/j.jpowsour.2005.09.008 (2006).
27. Largeot, C. *et al.* Relation between the ion size and pore size for an electric double-layer capacitor. *Journal of the American Chemical Society* **130,** 2730–2731; 10.1021/ja7106178 (2008).
28. Presser, V., Heon, M. & Gogotsi, Y. Carbide-Derived Carbons - From Porous Networks to Nanotubes and Graphene. *Adv. Funct. Mater.* **21,** 810–833; 10.1002/adfm.201002094 (2011).
29. Letellier, M. in *Encyclopedia of Spectroscopy and Spectrometry* (Elsevier2017), pp. 181–191.
30. Letellier, M., Chevallier, F. & Morcrette, M. In situ 7Li nuclear magnetic resonance observation of the electrochemical intercalation of lithium in graphite; 1st cycle. *Carbon* **45,** 1025–1034; 10.1016/j.carbon.2006.12.018 (2007).

31. Letellier, M. *et al.* The first in situ 7Li nuclear magnetic resonance study of lithium insertion in hard-carbon anode materials for Li-ion batteries. *The Journal of Chemical Physics* **118,** 6038–6045; 10.1063/1.1556092 (2003).
32. Fujimoto, H., Mabuchi, A., Tokumitsu, K., Chinnasamy, N. & Kasuh, T. 7Li nuclear magnetic resonance studies of hard carbon and graphite/hard carbon hybrid anode for Li ion battery. *Journal of Power Sources* **196,** 1365–1370; 10.1016/j.jpowsour.2010.09.026 (2011).
33. Tatsumi, K. *et al.* Low temperature 7Li-NMR investigations on lithium inserted into carbon anodes for rechargeable lithium-ion cells. *Journal of Power Sources* **81-82,** 397–400; 10.1016/S0378-7753(99)00114-7 (1999).
34. Gotoh, K. *et al.* Properties of a novel hard-carbon optimized to large size Li ion secondary battery studied by 7Li NMR. *Journal of Power Sources* **162,** 1322–1328; 10.1016/j.jpowsour.2006.09.001 (2006).
35. Qiu, S. *et al.* Manipulating Adsorption–Insertion Mechanisms in Nanostructured Carbon Materials for High-Efficiency Sodium Ion Storage // Manipulating Adsorption-Insertion Mechanisms in Nanostructured Carbon Materials for High-Efficiency Sodium Ion Storage. *Advanced Energy Materials* **7,** 1700403; 10.1002/aenm.201700403 (2017).
36. Dash, R. *et al.* Titanium carbide derived nanoporous carbon for energy-related applications. *Carbon* **44,** 2489–2497; 10.1016/j.carbon.2006.04.035 (2006).
37. Thommes, M. *et al.* Physisorption of gases, with special reference to the evaluation of surface area and pore size distribution (IUPAC Technical Report). *Pure and Applied Chemistry* **87,** 1051–1069; 10.1515/pac-2014-1117 (2015).
38. Buiel, E., George, A. E. & Dahn, J. R. On the Reduction of Lithium Insertion Capacity in Hard-Carbon Anode Materials with Increasing Heat-Treatment Temperature. *J. Electrochem. Soc.* **145,** 2252–2257; 10.1149/1.1838629 (1998).
39. Saurel, D. *et al.* A SAXS outlook on disordered carbonaceous materials for electrochemical energy storage. *Energy Storage Materials* **21,** 162–173; 10.1016/j.ensm.2019.05.007 (2019).
40. Yang, C.-P., Yin, Y.-X., Zhang, S.-F., Li, N.-W. & Guo, Y.-G. Accommodating lithium into 3D current collectors with a submicron skeleton towards long-life lithium metal anodes. *Nature Communications* **6,** 8058; 10.1038/ncomms9058 (2015).
41. Yang, G. *et al.* Insights into Lithium and Sodium Storage in Porous Carbon. *Nano Letters*; 10.1021/acs.nanolett.0c00943 (2020).
42. Stevens, D. A. & Dahn, J. R. The Mechanisms of Lithium and Sodium Insertion in Carbon Materials. *J. Electrochem. Soc.* **148,** A803; 10.1149/1.1379565 (2001).
43. Bonino, F. A Polymeric Electrolyte Rechargeable Lithium Battery. *J. Electrochem. Soc.* **135,** 12–15; 10.1149/1.2095538 (1988).
44. Tatsumi, K. *et al.* 7Li -Nuclear Magnetic Resonance Observation of Lithium Insertion into Mesocarbon Microbeads. *J. Electrochem. Soc.* **143,** 1923–1930; 10.1149/1.1836926 (1996).

45. Chevallier, F., Poli, F., Montigny, B. & Letellier, M. In situ7Li nuclear magnetic resonance observation of the electrochemical intercalation of lithium in graphite: second cycle analysis. *Carbon* **61,** 140–153; 10.1016/j.carbon.2013.04.078 (2013).
46. Boehm, H. P., Setton, R. & Stumpp, E. Nomenclature and terminology of graphite intercalation compounds (IUPAC Recommendations 1994). *Pure and Applied Chemistry* **66,** 1893–1901; 10.1351/pac199466091893 (1994).
47. Zaghib, K. *et al.* 7Li - NMR of Well-Graphitized Vapor-Grown Carbon Fibers and Natural Graphite Negative Electrodes of Rechargeable Lithium-Ion Batteries. *J. Electrochem. Soc.* **146,** 2784–2793; 10.1149/1.1392009 (1999).
48. Weiss, A. G. S. Carter, L. H. Bennett, D. J. Kahan: Metallic Shifts in NMR, A review of theory and comprehensive critical data compilation of metallic materials. Part I-IV (Progress in Materials Science, Vol. 20, Editors: B. Chalmers, J. W. Christian, T. B. Massals. *Berichte der Bunsengesellschaft für physikalische Chemie* **81,** 779–780; 10.1002/bbpc.19770810824 (1977).
49. Chevallier, F. *et al.* In Situ 7Li-Nuclear Magnetic Resonance Observation of Reversible Lithium Insertion into Disordered Carbons. *Electrochemical and Solid-State Letters* **6,** A225; 10.1149/1.1612011 (2003).
50. Yeon, S.-H., Jung, K.-N., Yoon, S., Shin, K.-H. & Jin, C.-S. Electrochemical performance of carbide-derived carbon anodes for lithium-ion batteries. *Journal of Physics and Chemistry of Solids* **74,** 1045–1055; 10.1016/j.jpcs.2013.02.028 (2013).
51. Bijoy, T. K. & Murugan, P. Lithiation of the Two-Dimensional Silicon Carbide–Graphene van der Waals Heterostructure: A First Principles Study. *J. Phys. Chem. C* **123,** 10738–10745; 10.1021/acs.jpcc.8b12492 (2019).
52. Ghimbeu, C. M. *et al.* Insights on the Na+ ion storage mechanism in hard carbon: Discrimination between the porosity, surface functional groups and defects. *Nano Energy* **44,** 327–335; 10.1016/j.nanoen.2017.12.013 (2018).
53. Kotina, I.M. *et al.* Study of the lithium diffusion in nanoporous carbon materials produced from carbides. *Journal of Non-Crystalline Solids* **299-302,** 815–819; 10.1016/S0022-3093(01)01124-3 (2002).
54. Hippauf, F. *et al.* Overcoming binder limitations of sheet-type solid-state cathodes using a solvent-free dry-film approach. *Energy Storage Materials* **21,** 390–398; 10.1016/j.ensm.2019.05.033 (2019).
55. Shen, Y., Qian, J., Yang, H., Zhong, F. & Ai, X. Chemically Prelithiated Hard-Carbon Anode for High Power and High Capacity Li-Ion Batteries. *Small (Weinheim an der Bergstrasse, Germany)* **16,** e1907602; 10.1002/smll.201907602 (2020).
56. Holtstiege, F., Schmuch, R., Winter, M., Brunklaus, G. & Placke, T. New insights into pre-lithiation kinetics of graphite anodes via nuclear magnetic resonance spectroscopy. *Journal of Power Sources* **378,** 522–526; 10.1016/j.jpowsour.2017.12.069 (2018).

57. Borchardt, L., Oschatz, M., Paasch, S., Kaskel, S. & Brunner, E. Interaction of electrolyte molecules with carbon materials of well-defined porosity: characterization by solid-state NMR spectroscopy. *Physical chemistry chemical physics : PCCP* **15,** 15177–15184; 10.1039/c3cp52283k (2013).

Acknowledgments

This research is funded by the European Social Fund and co-financed by tax funds based on the budget approved by the members of the Saxon State Parliament. This work was supported by the Fraunhofer and Max Planck cooperation programme.

The authors are thankful to Daniel Werner (Max Planck Institute of Colloids and Interfaces, Potsdam) for conducting the SAXS measurements and to Dr. Tobias Heil (Max Planck Institute of Colloids and Interfaces, Potsdam) and Dr. Jörg Kaspar (Fraunhofer Institute IWS, Dresden) for performing the Transmission Electron Microscopy. Rene Zenner (Fraunhofer Institute IWS, Dresden) is acknowledged for designing and constructing the graphic for proposed cluster formation mechanism. The authors thank Susann Kleber (Fraunhofer Institute IWS, Dresden) for performing the Raman measurements.

Author information:

Affiliations:

[a] Technical University Dresden, Chair of Inorganic Chemistry I, Bergstraße 66, 01069 Dresden, Germany

[b] Fraunhofer Institute for Material and Beam Technology IWS, Winterbergstr. 28, 01277 Dresden, Germany

[c] Technical University Dresden, Chair of Bioanalytical Chemistry, Bergstraße 66, 01069 Dresden, Germany

[d] Max Planck Institute of Colloids and Interfaces, Dept. of Colloid Chemistry, Am Mühlenberg 1, 14476 Potsdam, Germany

[e] Friedrich-Schiller-University Jena, Institute for Technical Chemistry and Environmental Chemistry, Center for Energy and Environmental Chemistry Jena (CEEC Jena), Philosophenweg 7a, 07743, Jena, Germany

Contributions:

L. M. Bloi performed the battery experiments, designed NMR measurement preparation, analysed data and wrote the manuscript. F. Hippauf and T. Boenke assisted in conception of experiments and substantially edited the manuscript. M. Rauche and S. Paasch performed the ^{7}Li NMR measurements and assisted with the interpretation of the results. K. Schutjajew analysed the SAXS data and conducted the XRD experiments. F. Schwotzer performed all SEM measurements and assisted in interpretation of data. J. Pampel, S. Dörfler, H. Althues and M. Oschatz conceived the project and edited the manuscript.

S. Dörfler, H. Althues and M. Oschatz discussed the results and implications of the project. E. Brunner and S. Kaskel supervised the project and commented on the manuscript.

Corresponding author:
Correspondence to Stefan Kaskel (*E-mail: stefan.kaskel@tu-dresden.de).

Competing interests:

The authors declare no competing financial or non-financial interests.

Supplementary Information:

Supplementary Tables 1-2, Figures 1-4, Notes and references.